Ceramide induces early and late apoptosis in human papilloma virus$^+$ cervical cancer cells by inhibiting reactive oxygen species decay, diminishing the intracellular concentration of glutathione and increasing nuclear factor-κB translocation

Gisela Gutiérrez[a,d], Criselda Mendoza[b], Luis F. Montaño[c] and Rebeca López-Marure[a]

Ceramide is regarded as an important cellular signal for the induction of cell death. We have previously shown that ceramide induces the death of cervical tumor cells without biochemical and morphological markers of apoptosis. The mechanisms by which ceramide induces cell death are not understood, therefore we evaluated the effect of C6-ceramide, a synthetic cell-permeable analog of endogenous ceramides, in signaling pathways involved in the oxidative stress of three cervical human papilloma virus$^+$ cancer cell lines. Reactive oxygen species production was determined by fluorescent 2,7-dichlorofluorescein, nitrite concentration by the Griess reaction (as an indirect measure of nitric oxide production), mitochondrial membrane potential by staining with Rh123, reduced-glutathione concentration by high-pressure liquid chromatography, nuclear factor-κB translocation by electrophoretic mobility shift assay, inhibitory protein of nuclear factor-κB expression by Western blot and cell death by a poly-caspases fluorochrome-labeled inhibitors of caspases apoptosis assay. C6-ceramide induced early and late apoptosis, which was associated with an increase in reactive oxygen species and nitric oxide production, a loss in mitochondrial membrane potential, an increase in nuclear factor-κB translocation, and a decrease in reduced glutathione concentration. C6-ceramide did not modify the expression of inhibitory protein of nuclear factor-κB and its antiproliferative effect was not abrogated by Bay 11-7082, an inhibitory protein of nuclear factor-κB kinase inhibitor. Our results suggest that oxidative stress might participate in the ceramide-induced damage to human papilloma virus$^+$ cervical cancer cells. *Anti-Cancer Drugs* 18:149–159 © 2007 Lippincott Williams & Wilkins.

Anti-Cancer Drugs 2007, **18:**149–159

Keywords: cervical cancer, early and late apoptosis, inhibitory protein of nuclear factor-κB, nuclear factor-κB, nitric oxide, reactive oxygen species, reduced glutathione

[a]Department of Cell Biology, National Institute of Cardiology, Ignacio Chávez, [b]Investigation Center of Infectious Diseases, INER, Mexico. [c]Laboratory of Immunology, Department of Biochemistry, School of Medicine, UNAM, Mexico and [d]Department of Urology and Gynecology, Children's Hospital of Mexico, "Federico Gómez".

Correspondence to R. López-Marure, Departamento de Biología Celular, Instituto Nacional de Cardiología 'Ignacio Chávez'. Juan Badiano No. 1, Colonia Sección 16, Tlalpan, CP 14080, Mexico DF, Mexico.
Tel: +52 55 73 29 11 ext. 1337; fax: +52 55 73 09 26;
e-mail: rlmarure@yahoo.com.mx

Sponsorship: G.G. (postgraduate student from the Instituto Politécnico Nacional) was supported by CONACyT-143675 scholarship.

Received 19 May 2006 **Revised form accepted** 27 September 2006

Introduction

Ceramide, which is the product of the hydrolysis of sphingomyelin or is synthesized from serine and palmitate in a de-novo pathway, plays a critical role in apoptosis, cell proliferation, cellular senescence and gene regulation through the activation of transcription factors such as nuclear factor (NF)-κB [1,2]. Ceramide induces the generation of reactive oxygen species by interacting with the complex III of the mitochondria electron transport chain [3]. Ceramide induces NF-κB and activating protein-1 (AP-1) translocation [4,5].

The major physiological source of reactive oxygen species (ROS) is mitochondrial respiration [6]. ROS activate NF-κB and AP-1, both of which can signal apoptosis, similarly to ceramide [7–9]. The mitochondrial production of ROS is regulated by antioxidant enzymes such as phospholipid hydroperoxide glutathione peroxidase, glutathione peroxidase and manganese superoxide dismutase [7]. Reduced glutathione (GSH) is the only mitochondrial defense against peroxides generated from the electron transport chain through the GSH redox cycle.

Uterine cervical cancer is the second most important cause of death in Mexican women [10]. It was previously we found that ceramide promotes the death of human cervical tumor cells in the absence of biochemical and morphological markers of apoptosis [11], although the

0959-4973

mechanism by which ceramide exerts such cellular effects is unknown. Hence, in this work we analyzed possible pathways involved in ceramide-induced death such as ROS, nitric oxide (NO), GSH, NF-κB, inhibitory protein of NF-κB (IκB-α) and mitochondrial membrane potential in human papilloma virus (HPV)$^+$ CaLo, InBl and HeLa cell lines, which derive from human cervical cancers [12,13]. Our results showed that ceramide induced early and late apoptosis by increasing ROS and NO production, reducing GSH levels, inducing NF-κB translocation, and a loss in the mitochondrial membrane potential. IκB-α expression was not modified.

Methods

Materials

Fetal bovine serum (FBS) was purchased from Gibco/BRL (Grand Island, New York, USA). Hematoxylin, OG6 dye and EA50 were from Merck (New Jersey, USA). 2,7-Dichlorofluorescein diacetate (DCFDA) was purchased from Molecular Probes (Eugene, Oregon, USA). The Bio-Rad protein assay was purchased from Bio-Rad (Hercules, California, USA). Griess reagent was purchased from ICN (Costa Mesa, California, USA). Sterile plastic material for tissue culture was from Nunc and Costar. [γ-^{32}P]ATP was purchased from Perkin-Elmer (Boston, Massachusetts, USA), T4 polynucleotide kinase from New England Biolabs (Beverley, Massachusetts USA) and poly dI–dC from Amersham Pharmacia (Uppsala, Sweden). The ^{32}P-labeled double-stranded oligonucleotides were from Santa Cruz (Santa Cruz, California, USA). IκB-α kinase inhibitor Bay 11-7082 was from Calbiochem (La Jolla, California, USA) and FAM-fluorochrome-labeled inhibitors of caspases (FLICA) poly caspase detection kit was from Serotec (Raleigh, North Carolina, USA). C6 and all other chemicals were purchased from Sigma-Aldrich (St Louis, Missouri, USA).

Cell culture

CaLo and InBl cells were obtained from cervical cancer biopsies. CaLo cells derived from an in-situ carcinoma are clinically characterized as II-B and are HPV-18$^+$, whereas InBl cells derived from a metastasic cervical tumor are IV-A and HPV-18$^+$ [12,13]. HPV-18$^+$ HeLa cells were purchased from the American Type Culture Collection (ATCC; Manassas, Virginia, USA). All tumor cell lines were cultured in RPMI-1640 medium supplemented with 5% FBS and L-glutamine (2 mmol/l). All experiments were performed in cultures plated at a cell density of 2×10^3 cells/cm^2.

Cell morphology

Papanicolaou staining was used to determine modifications in the cellular morphology at different culture times [14]. 2×10^4 cells were plated on glass slides with or without 3 μmol/l C6, washed twice with phosphate-buffered saline (PBS) and fixed in 96% ethanol. To hydrate, glass slides were incubated in ethanol at different concentrations (96, 70, 50 and 0%) for 5, 1, 1 and 3 min, respectively. After rehydration, the cells were stained with hematoxylin for 1.5 min and washed three times with deionized water. To dehydrate the cells, the slides were incubated in ethanol at increasing concentrations of 50, 70 and 96% for 1 min each. Cells were then stained with the OG6 dye for 5 min and fixed in 96% ethanol for 1 min. Then, cells were stained with EA_{50} for 5 min, fixed again in 96% ethanol for 3 min and placed in ethanol–xylol (1 : 1 v : v). Slides were mounted and the morphology was analyzed by light microscopy. Micrographs were obtained with a final magnification factor of × 100.

Cell death detection

Cell death was detected using the carboxyfluorescein FLICA apoptosis detection kit (Serotec) that determines caspase activation. Cells were cultured with or without C6 for 24 h. At the end, cells were recovered from the culture plate, and were adjusted to a final concentration of 3×10^6 cells/ml in *N*-2-hydroxyl piperazine-*N*′-2-ehane sulfonic acid (HEPES buffer) before transferring 300 μl of each cell suspension to sterile tubes in which 10 μl of a 30 × FLICA solution was added. The tubes were protected from light, manually agitated and incubated for 1 h at 37°C in a 5% CO_2 atmosphere. At the end of the incubation, 2 ml of the 1 × wash buffer was added to each tube. Cells were mixed and centrifuged at 1200 r.p.m. for 5 min at room temperature. The cell pellet was resuspended in 1 ml of the 1 × wash buffer, centrifuged and the pellet was resuspended in 400 μl of the 1 × wash buffer. Cells were then stained with 2 μl of propidium iodide (PI) (250 μg/ml) and analyzed with a flow cytometer using the Cell Quest software program (Becton Dickinson, San Jose, California, USA).

Measurement of reactive oxygen species

ROS generation in tumor cells was assessed using DCFDA, a nonfluorescent probe, which upon oxidation by ROS and peroxides is converted to the highly fluorescent derivative DCF [15,16]. Cells were incubated with DCFDA (10 μmol/l) for 30 min at 37°C and washed twice with PBS. Tumoral cell lines were then cultured in the absence or presence of C6 for 20, 40 and 60 min. After an extensive wash, fluorescence was evaluated in the FACSCalibur (Becton Dickinson). The mean intensity of the green fluorescence was determined using the Cell Quest software program and expressed as fluorescence units. Fluorescence was measured using an excitation wavelength of 480 nm, a dichromic mirror with a 505-nm long pass and emitter bandpass of 535 nm (Chroma Technology, Rockingham, Vermont, USA) using neutral density filters to attenuate the excitation light.

Quantification of nitrite

Cells were seeded in 96-well plates (Nunc) at a density of 1×10^5 cells/well in RPMI without phenol red, 5% FBS,

and with or without 3 μmol/l C6. After 24 h, 100 μl of the conditioned medium was diluted 1 : 1 with 100 μl of Griess reactive and incubated for 15 min at room temperature. Previously, a standard curve was performed using known concentrations of nitrite (range 0.4–100 μmol/l). The optical density of the plates was measured at 540 nm in a multiplate spectrophotometer. The absorbance of the concentrations of control and problem samples was plotted against the standard curve [17].

Determination of mitochondrial membrane potential

The changes in mitochondrial membrane potential were examined by monitoring the staining with rhodamine 123 (Rh123), a lipophilic cation selectively taken up by mitochondria, and whose uptake is directly proportional to mitochondrial $\Delta\Psi$ [18]. After treatment with C6, cells were stained with Rh123 (0.2 μg/ml) for 10 min. The fluorescence intensity was analyzed with a flow cytometer (FACSCalibur) using the Cell Quest software program.

Determination of glutathione by high-pressure liquid chromatography

Ten milligrams of protein were placed in an eppendorff tube, and 500 μl of sulfonic acid (200 mmol/l) and diethylenetriaminepentacetic acid 5 mmol/l were added. The solution was vortexed for 1 min and centrifuged at 13 000 r.p.m. (4°C) during 30 min. The supernatant was diluted 1 : 1 with the high-pressure liquid chromatography (HPLC) mobile phase (containing monobasic sodium phosphate 50 mmol/l, octasulfonic acid 0.05 mmol/l at pH 3 adjusted with phosphoric acid) and was filtered with a membrane of 45 μm. Twenty microliters was injected into the HPLC (Waters 600, Arcade, New York, USA) previously connected to an electrochemical detector with a potential of + 850 mV in pulse mode, with a 1-ml/min flow in the mobile phase. Previously, a standard curve was performed using known concentrations of GSH (concentration vs. area). To calculate the concentrations of GSH, the corresponding areas to the samples were calculated by interpolation [19].

Cytoplasmic and nuclear protein extraction

Cytoplasmic and nuclear protein was obtained as previously described [20]. Three million tumor cells were seeded in 100-mm diameter Petri dishes and treated with 3 μmol/l C6 for 30 min, thereafter cells were scraped with a rubber policeman in PBS, collected and centrifuged at 3000 r.p.m. for 5 min. The pellet was frozen in liquid nitrogen for 15 s and resuspended gently in 100 μl of hypotonic solution [10 mmol/l HEPES pH 7.9, 10 mmol/l KCl, 1.5 mmol/l $MgCl_2$, 1 mmol/l dithiothreitol (DTT)]. Nuclei were stained with a trypan blue solution and observed under the microscope to evaluate their integrity. Nuclei were collected by centrifugation at 3500 r.p.m. for 10 min at 4°C, and the supernatant containing cytoplasmic protein was collected and kept at −20°C. The pellets were resuspended in 15 μl of hypertonic solution [10 mmol/l HEPES pH 7.9, 0.4 mol/l NaCl, 1.5 mmol/l $MgCl_2$, 25% glycerol, 0.2 mmol/l ethylenediaminetetracetic acid (EDTA), 1 mmol/l DTT, 0.5 mmol/l phenylmethylsulfonyl fluoride (PMSF)], incubated for 30 min with gentle mixing at 4°C and centrifuged at 14 000 r.p.m. for 20 min. The resultant supernatant containing the nuclear protein was collected, diluted 1 : 1 with an HDKE buffer (20 mmol/l HEPES pH 7.9, 50 mmol/l KCl, 25% glycerol, 0.2 mmol/l EDTA, 1 mmol/l DTT, 0.5 mmol/l PMSF) and stored at −70°C. Total nuclear protein concentration was determined using the Bio-Rad protein assay.

Electrophoretic mobility shift assay

Nuclear protein extracts (10 μg) were assayed for DNA interaction by electrophoretic mobility shift assay as described previously [21]. The ^{32}P-labeled double-stranded oligonucleotides (5′-AGTTGAGGGGACTTTCCCAGGC-3′) contain the NF-κB consensus sequence or the mutated sequence (5′-AGTTGAGGC-GACTTTCCCAGGC-3′). The binding reactions were carried out by incubating the samples in a reaction buffer (50 mmol/l KCl, 20% glycerol, 0.2 mmol/l EDTA, 1 mmol/l DTT, 0.5 mmol/l PMSF, 20 mmol/l HEPES, pH 7.9, 1 μg/μl bovine serum albumin, 1 μg/μl poly dI–dC). DNA–protein complexes were resolved on 5% polyacrylamide gel at 100 V during 2 h. The gel was dried and exposed to a Storage Phosphor Screen (Molecular Dynamics, San Francisco, California, USA) that was read in a Storm 850 Phosphorimager (Molecular Dynamics) and analyzed with ImageQuant software (Molecular Dynamics). Cold competition assays were conducted by adding a 100-fold molar excess of homologous unlabeled NF-κB consensus sequence.

Western blot

One hundred and fifty micrograms of cytoplasmic protein was loaded per lane, resolved by sodium dodecyl sulfate–polyacrylamide gel electrophoresis on 7.5% polyacrylamide gels, and transferred to nitrocellulose membranes. The membranes were blocked with a suspension of 5% fat-free milk powder in 20 mmol/l Tris, 137 mmol/l NaCl, 3 mmol/l KCl and 0.1% Tween-20 pH 7.6 (TBS-T), and incubated for 2 h with an anti-IκB-α (diluted 1 : 500) or antiβ-actin (1 : 5000) monoclonal antibody. The blots were washed for 5 min in TBS-T twice, before a peroxidase goat antimouse antibody diluted 1 : 2500 was added for 30 min. At the end, the blots were washed twice with TBS-T and peroxidase was detected using a chemiluminiscent system.

Cell proliferation

The number and viability of cells was evaluated by crystal violet staining [22]. Briefly, cells were seeded in 96-multiwell culture plates and were treated with 3 μmol/l

C6, or different concentrations of Bay 11-7082, or both, for 48 h. At the end of these treatments, cells were fixed with 100 µl of ice-cold glutaraldehyde [1.1% in PBS (150 mmol/l NaCl, 30 mmol/l KCl, 15 mmol/l Na_2HPO_4, 2 mmol/l KH_2PO_4 pH 7.4)] for 15 min at 4°C. Plates were washed three times by submersion in deionized water, air-dried and stained for 20 min with 100 µl of a 0.1% crystal violet solution (in 200 mmol/l formic acid buffer at pH 6). After careful aspiration of the crystal violet solution the plates were extensively washed with deionized water and air-dried before the solubilization of the bound dye with 100 µl of a 10% acetic acid solution incubated during 30 min. The optical density of the plates was measured at 595 nm in a multiplate spectrophotometer.

Statistical analysis

Results are presented as mean ± standard deviation. All experiments were performed in triplicate and were repeated at least three times. Student's *t*-test was applied to determine statistical significance with a $P < 0.01$.

Results

Ceramide induced morphological changes

As ceramide induces death in several cell types including tumor cells [23], we evaluated the morphological changes induced by short incubation periods with C6 of three HPV^+ cell lines (CaLo, InBl and HeLa, obtained from cervical uterine cancer patients), to determine the time that the cell takes to show serious damage and to present morphological changes. The Papanicolaou staining of all non-C6-treated tumor cells showed a classical tumoral morphology with large nuclei, and a dense and well distributed chromatin, homogeneous cytoplasm, and pleomorphism (Fig. 1, controls). The three cell lines treated for 6 h with C6 showed a reduced cell size, a compact cytoplasm, condensation of the chromatin, and strong nuclear staining (Fig. 1). Only InBl cells showed an elongated shape. The morphological changes in HeLa cells treated with C6 were smaller than in CaLo and InBl cells. An evident detachment of the cells was observed after 12 h of treatment with C6 (data not shown). The cytoplasm and nuclei changes are characteristic of necrosis.

Ceramide induced early and late apoptosis

We previously showed that ceramides induce death, in the absence of biochemical and morphological markers of apoptosis [11]. To determine the type of cell death induced by C6, we evaluated the activation of caspases by using the carboxyfluorescein FLICA apoptosis detection kit. Flow cytometry analysis of cells labeled with both FLICA and PI (Fig. 2a) showed an increase in the percentage of FLICA-positive cells (early apoptosis) as well as in the percentage of FLICA and PI-positive cells (late apoptosis) in the cell lines treated with C6 in comparison with untreated cells. It was interesting to observe that the percentage of cells in late apoptosis was significantly higher than the increase observed for early apoptosis (Fig. 2b).

Ceramide induced formation of reactive oxygen species and nitrite

Ceramide-induced ROS production is associated to cell death and ceramide-induced cytotoxicity is often directly attributed to NO [24,25]. Therefore, we determined the effect of C6 in ROS and nitrite production at different times. C6 did not alter ROS concentration after 20 and 40 min of treatment; however, it induced an increase in ROS concentration of 48, 33 and 53% in CaLo, InBl and HeLa cells, respectively, after 60 min in comparison with untreated control cells (Table 1). Peroxide, which was used as a positive control to induce ROS, increased ROS production by 2-fold at all the times tested and in all the cell lines.

C6 exposure induced a significant rise of NO concentration in all cell lines (Fig. 3). We observed a 3.9-fold induction in HeLa cells, and more than a 4-fold induction in CaLo and InBl cells. The maximal increase was observed after 60 min of treatment. Shorter and longer exposure times did not have a significant difference in comparison with untreated cells (data not shown).

Ceramide induced a loss of the mitochondrial membrane potential

Mitochondrial dysfunction has been implicated in the decrease of transmembrane potential, the accumulation of ROS, the membrane permeability transition and the release of apoptotic factors during apoptosis or necrosis [26]. CaLo, InBl and HeLa cells treated with C6 had a decrease of 65, 36 and 36% in Rh123 uptake, respectively, in comparison with untreated tumoral cells that showed a high Rh123 uptake (Figs. 4a and b), thus indicating that C6 induces the loss of membrane potential and then the loss of membrane integrity.

Ceramide induced a decrease in reduced glutathione concentration

Apoptosis or necrosis can be induced by GSH depletion or destruction in several types of mammalian cells [26]; therefore, we assessed GSH concentration in cells treated with C6 after 6 h. The results showed that C6 induced a decrease in GSH concentration of 28, 17 and 46% in CaLo, InBl and HeLa cells, respectively, in comparison with untreated cells (Fig. 5).

Ceramide induced nuclear factor-κB translocation

NF-κB is one of the key regulatory molecules in the oxidative-stress-induced cell activation, and is directly influenced by reactive species and proinflammatory agents [27,28]. As we had observed a reduction of NO and ROS production in cells treated with C6, we evaluated NF-κB translocation. A faint basal translocation

Fig. 1

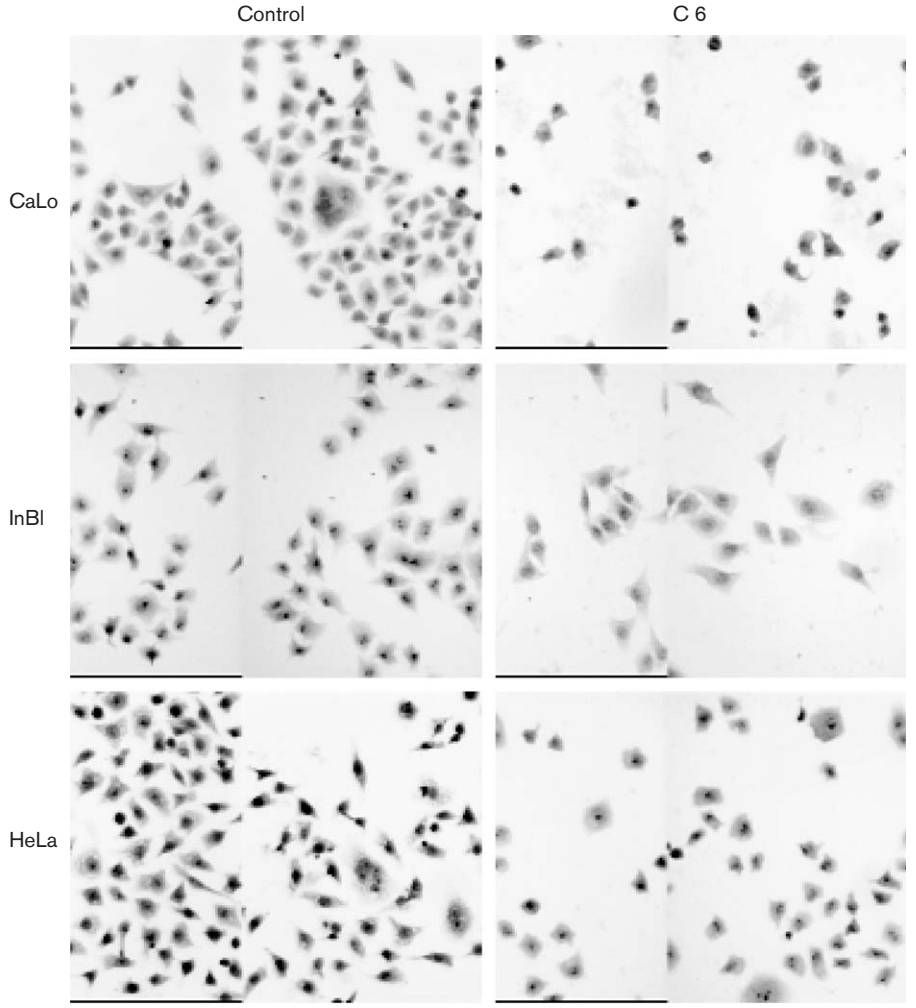

C6-ceramide-induced (C6) morphological changes. CaLo, InBl and HeLa cells were cultured with 3 μmol/l C6 for 3, 6, 12 and 24 h. Papanicolaou staining of the cells was performed as indicated in Methods. Light microscopy micrographs after a 6-h incubation period are shown; the photograph magnification is × 100.

of NF-κB was detected in all non-C6-treated control cells. C6-treated cells exhibited two nuclear complexes, which were named complex I and II in terms of their electrophoretic mobility. C6 induced a 4.5-, 3.1- and 1.6-fold increase in the nuclear NF-κB complex I in CaLo, InBl and HeLa cells, respectively (Fig. 6). C6 did not modify the NF-κB complex II. Competition experiments with cold NF-κB specific oligonucleotides confirmed the specificity of the DNA-binding activity (Fig. 6).

To determine whether NF-κB translocation was associated with the degradation of its inhibitor IκB-α, the expression of the latter was evaluated. As the Western blot pattern was not affected by C6 treatment, we conclude that C6 does not affect IκB-α degradation of the cell lines (Fig. 7).

To determine whether NF-κB translocation is important in the cell death induced by C6 or is a consequence of ROS generation, we used the IκB-α kinase inhibitor Bay 11-7082 to determine whether the inhibition of the proliferation induced by C6 was abrogated in CaLo cells. We found that Bay 11-7082, at different concentrations, did not affect the cell proliferation. When Bay 11-7082 was used in combination with C6, the C6-induced antiproliferative effect was not reverted (Fig. 8). Similar results were obtained with HeLa and InBl cells (data not shown).

Discussion

We previously demonstrated that ceramide induces cell death in several cervical cancer cells [11]. As the mechanism of action remains unclear, in this work we

Fig. 2

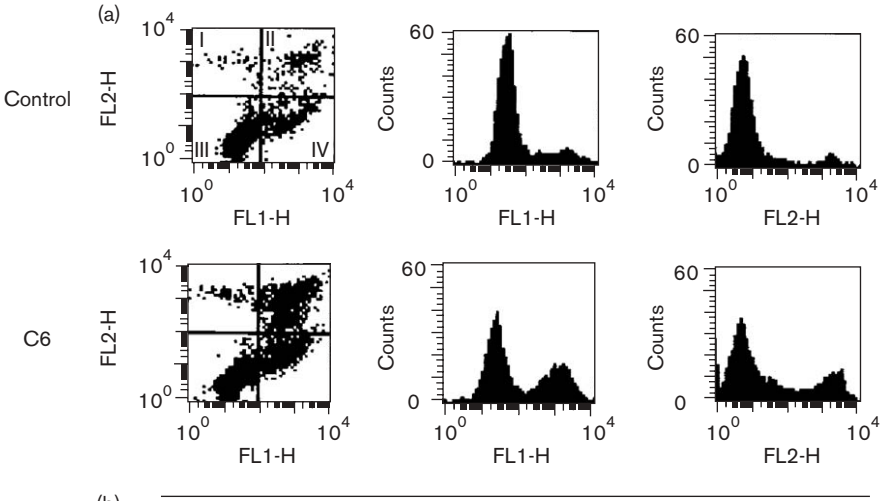

(b)

		Percentage of cells	
		Early apoptosis	Late apoptosis
CaLo	Control	11.48	1.42
	C6	7.2	11.64
InBl	Control	7.64	4.08
	C6	16.24	22.02
HeLa	Control	10.42	6.66
	C6	17.52	39.66

C6-ceramide (C6) induced early and late apoptosis. CaLo, InBl and HeLa cells were cultured with 3 μmol/l or without C6, and cell death was evaluated 24 h latter (see Methods). The results are shown as histograms in InBl cells (a) or as the percentage of dead cells in all cell lines used (b). The figure inside the quadrants in the histograms represent the following: I, PI-positive cells; II, late apoptotic cells; III, nonapoptotic and nonnecrotic cells; IV, early apoptotic cells.

Table 1 C6 induced an increase in ROS production. CaLo, InBl and HeLa cells were cultured with 3 μmol/l C6 or 2 μmol/l H_2O_2 for 20, 40 and 60 min.

Cell line	Fluorescence intensity (units)		
	20 min	40 min	60 min
CaLo			
control	26 424 ± 3252	24 734 ± 1998	20 033 ± 2190
C6	30 275 ± 2534	30 490 ± 2769	*29 784 ± 1956
H_2O_2	*112 004 ± 10 428	*57 434 ± 3552	*54 129 ± 4320
InBl			
control	71 898 ± 6453	64 932 ± 7564	57 266 ± 6423
C6	72 493 ± 8567	64 950 ± 4560	*76 428 ± 7564
H_2O_2	*2 56 931 ± 30 421	*1 74 593 ± 20 432	*1 23 493 ± 11 323
HeLa			
control	26 054 ± 3211	19 883 ± 2110	17 272 ± 2358
C6	27 054 ± 2851	*23 772 ± 2765	*26 524 ± 1789
H_2O_2	*76 142 ± 8563	*50 961 ± 6542	*38 644 ± 4251

ROS concentration was evaluated using DCFDA and flow cytometry (see Methods). Fluorescence intensity units were calculated multiplying the number of events by the mean of the fluorescence.
The results correspond to a representative experiment of three independent assays.
C6, C6-ceramide; H_2O_2, hydrogen peroxide (positive control); ROS, reactive oxygen species.
*$P < 0.01$ in comparison to control values.

tried to evaluate the type of cell death and some possible pathways that might be involved in the C6-induced cell death, in three HPV-18$^+$ cervical cancer cell lines.

To determine the time that C6 takes to induce damage, tumor cells were cultured with C6 and their morphology was then evaluated at different times. C6 caused a morphological damage in all tumor cells after 6 h of treatment. Evident cytoplasmic and nuclei characteristics of damage were observed (Fig. 1). These changes support the presence of a necrotic process and coincide almost entirely with our already reported results [11].

To determine the type of cell death induced by C6, we used a FLICA apoptosis detection kit to detect several active caspases. After 24 h of treatment with C6, the percentage of cells in early and late apoptosis was increased (Fig. 2). Late apoptosis is a synonym of secondary necrosis [29], and is defined by the presence of nuclear condensation and/or fragmentation along with

Fig. 3

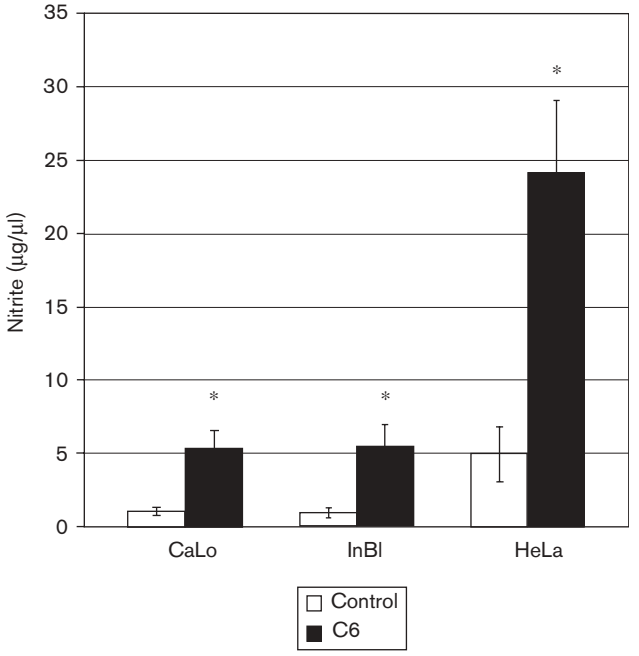

C6-ceramide (C6) induced an increase of nitrite concentration. CaLo, InBl and HeLa cells were cultured with 3 µmol/l C6 for 1 h. Nitrite concentration was determined by Griess reagent reactivity (see Methods). The results shown correspond to a representative experiment of three independent assays. *Indicates $P<0.01$ in comparison to control non-C6-treated cells.

PI uptake [29]. As our results showed that the majority of cells had nuclear condensation and PI uptake, we conclude that C6 induces two different types of cell death: early and late apoptosis. It has been shown that in C2-ceramide-induced cytotoxicity in NB16 neuroblastoma cells, there was 25% apoptotic death and that the majority of cells possessed necrotic morphology, and were Annexin V and PI positive (necrotic/late apoptotic fraction) [30], indicating that ceramide is able to induce apoptosis and necrosis in different cancer cells.

Nevertheless, in this work we did observe morphological changes associated with apoptotic death such as nuclear condensation; the difference with our previous report [11] might be that we evaluated the morphological changes at shorter periods of time. It is interesting to observe that C6 triggered early apoptosis in a fraction of the cells, but cell death was primarily caused by late apoptosis (Fig. 2). It is possible that cells treated with C6 for long periods of time (48 h) have an predominant cell death by late apoptosis and, therefore, no nuclei condensation, whereas early apoptosis might be accompanied by nuclei condensation.

Mammalian cell death can be induced through oxidative stress by ROS [25]. Our results showed that C6 induced an increase in ROS production in all the tumor cells (Table 1). Although ROS has been associated with apoptotic death [31], in the A172 human glioma cell, ceramide causes nonapoptotic cell death by inducing ROS generation [32].

Fig. 4

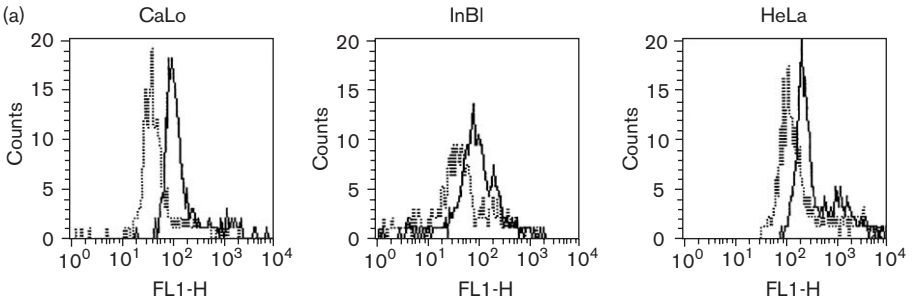

(b)

	Fluorescence intensity (units)	
	Control	C6
CaLo	94025 ± 8500	39309 ± 4300*
InBl	103569 ± 11420	66432 ± 5243*
HeLa	176434 ± 22568	112935 ± 10259*

C6-ceramide (C6) induced loss of mitochondrial membrane potential. CaLo, InBl and HeLa cells cultured with 3 µmol/l C6 for 3 h were stained with Rh123 (0.2 mg/ml) for 10 min. After extensive washing, Rh123 uptake was determined by flow cytometry as described in Methods. The results are shown as histograms (a) or as fluorescence intensity (b). In (a), the dotted line represents C6-treated cells and the continuous line nontreated cells (control). Fluorescence intensity units were calculated by multiplying the number of events by the mean of the fluorescence. The results correspond to a representative experiment of three independent assays and represent the mean ± the standard deviation of the mean. *Indicates $P<0.01$ in comparison to control non-C6-treated cells.

NO, synthesized from L-arginine by NO synthases, promotes apoptosis in some cells and inhibits it in others. This difference might be the consequence of the rate of NO production and the interaction of NO with biological molecules such as ROS [33]. The increase in ROS production that we observed was associated with a rise in nitrite concentration, indicating a possible increase of NO (Fig. 3). Overproduction of NO acts as a proapoptotic modulator; however, low or physiological concentrations of NO prevent cells from apoptosis [34]. In CCK-8-induced pancreatic hypoplasia, it has been shown that endogenously synthesized NO suppresses apoptosis, but increases cell death along nonapoptotic pathways [35]. It is possible that the increase in the nitrite concentration in cervical tumor cells treated with C6 is associated to a nonapoptotic cell death.

Fig. 5

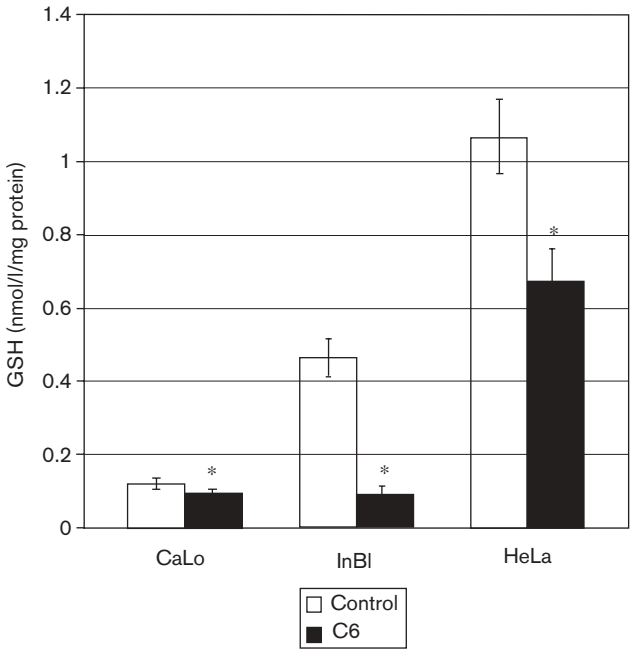

C6-ceramide (C6) decreased reduced glutathione (GSH) concentration. CaLo, InBl and HeLa cells were cultured with 3 μmol/l C6 for 3 h before GSH concentration was determined by high-pressure liquid chromatography (see Methods). The results shown correspond to a representative experiment of three independent assays. *Indicates a $P<0.01$ in comparison to control cells.

Mitochondria are one of the most important cellular sources of ROS owing to their quantitative consumption of molecular oxygen. ROS cause peroxidation of membrane lipids, cleavage of mitochondrial DNA and impairment of ATP generation, with the resulting irreversible damage to mitochondria [7]. C6 induced a loss of the mitochondrial membrane potential indicating mitochondrial damage (Fig. 4). Contrary to our results, Kim *et al.* (2005) [32] showed that ceramide causes ATP depletion, without loss of mitochondrial membrane potential, and a nonapoptotic cell death in A172 human glioma cells, indicating that ceramide can induce differential effects depending on the cell type used. The loss of the mitochondrial membrane potential of all the cell lines we tested, in association with our previous observations of a decrease in the 3-(4,5-dimethylthiazol-2yl)-2,5-diphenyl tetrazolium bromide reduction [11], suggest an important role of the mitochondria in the C6-induced cell death in cervical tumor cells.

As glutathione is the major nonprotein antioxidant in mitochondria that protects the cell from oxidative stress by metabolizing hydrogen peroxide [36,37], it can inhibit both apoptosis and necrosis. C6 induced a decrease in the GSH concentration of the cervical cancer cell lines evaluated (Fig. 5). In other cell lines such as U937 monocytes and Jurkat T cells, the growth arrest and apoptosis induced by C2 and/or C6 ceramide are

Fig. 6

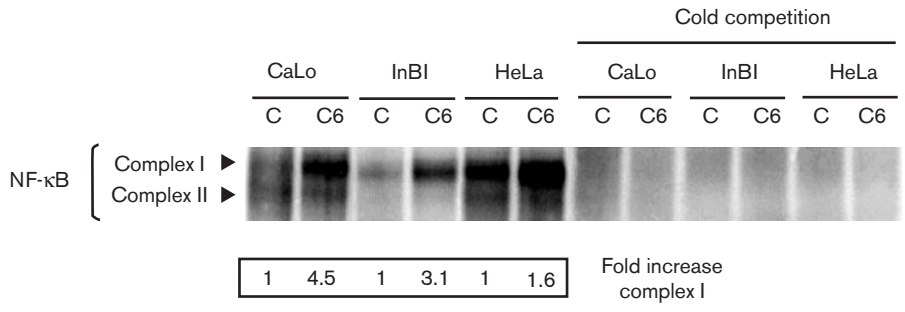

C6-ceramide (C6)-induced nuclear factor-κB (NF-κB) translocation. CaLo, InBl and HeLa cells were cultured with 3 μmol/l or without C6. NF-κB translocation was evaluated after 30 min in nuclear protein extracts (10 μg) by electrophoretic mobility shift assay as described in Methods. NF-κB complex I and II are shown according to their electrophoretic mobility in 7.5% acrylamide gels. The specificity of NF-κB was tested by adding to nuclear extracts a 100-fold molar of a cold NF-κB oligonucleotide (Cold competition). The results shown correspond to a representative experiment of three independent assays. C, control non-C6-treated cells.

Fig. 7

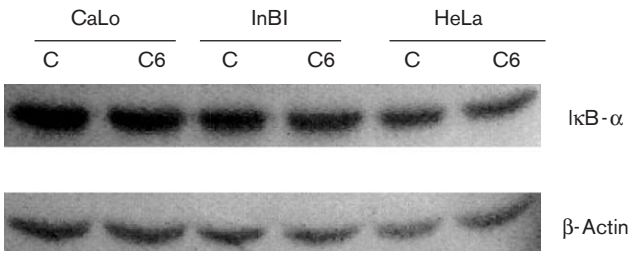

C6-ceramide (C6) did not modify the expression of IκB-α protein. CaLo, InBl and HeLa cells were cultured with 3 μmol/l or without C6. Inhibitor protein of nuclear factor-κB expression was evaluated after 30 min in cytoplasmic protein extracts (150 μg) by Western blot (see Methods). β-Actin was used as a load control. The results shown correspond to a representative experiment of three independent assays. C, control non-C6-treated cells.

Fig. 8

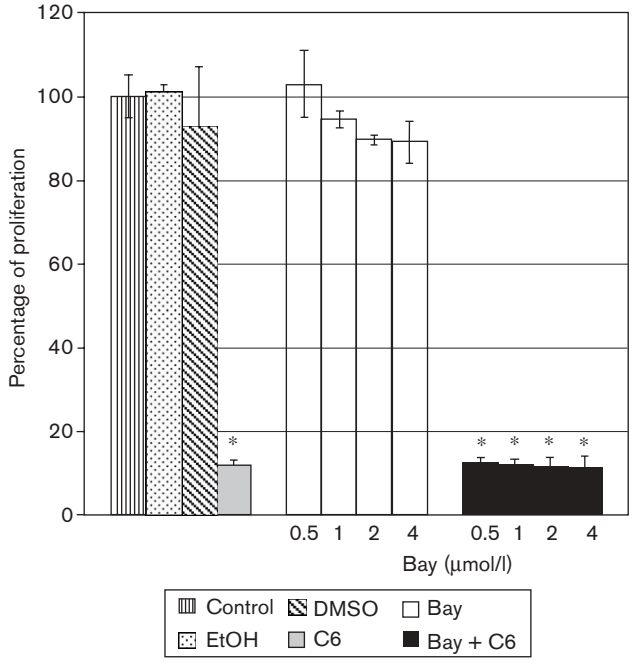

C6-ceramide (C6)-induced antiproliferative effect was not abrogated by an inhibitor protein of nuclear factor-κB kinase inhibitor. CaLo, InBl and HeLa cells were cultured with different concentrations of Bay 11-7082 alone or in combination with 3 μmol/l C6 and cell proliferation was evaluated 48 h later (see Methods). C_2H_5OH (ethanol) and DMSO (dimethyl sulfoxide), which were used as vehicles of C6 and Bay 11-7082, respectively, served as controls. The results shown correspond to a representative experiment of three independent assays. *Indicates a $P<0.01$ in comparison to control cells.

preceded by a rise in mitochondrial peroxide production, and a large time- and dose-dependent loss of cellular glutathione [31]. In lung epithelial cells, depletion of glutathione results in ceramide accumulation [38]. Our results suggest that GSH depletion, induced by the addition of exogenous ceramide, may be the link between oxidative stress and C6-mediated nonapoptotic cell death in cervical cancer. Our results strongly suggest that the initial ROS increase is accompanied by an increase in GSH, but after 60 min of culture time, ceramide-treated cells show a decrease in GSH concentration and therefore a relative increase in ROS, which could explain the cell damage induced by ceramide. It has been shown that the acidic sphingomyelinase, an enzyme responsible for the production of ceramide by sphingomyelinase hydrolysis, induces the production of ROS, accompanied by mitochondrial depolarization and GSH depletion, as a result of the targeting of mitochondria, in the apoptosis of ceramide-treated rat hepatocytes [39]. It would be interesting to evaluate the activation of acidic sphingomyelinase in C6-treated cervical tumor cells.

Sphingomyelinase and its product ceramide induce the activation of NF-κB [40], and it is well known that ROS produced in mitochondria activate transcription factors such as NF-κB [7]. As we observed an increase in ROS in C6-treated cells, we evaluated the translocation of NF-κB in these cells. The results presented here show that C6 induces the translocation of NF-κB in all cell lines (Fig. 6). Other works have shown that C2- and C6-ceramides induce NF-κB translocation that has been associated with apoptosis in HCT116 and OVCAR-3 cancer cells [41]. Similarly, an increased ceramide synthesis has been associated with the inhibition of AP-1 and NF-κB transactivation in macrophages [42]. We have previously shown a marked decrease in NF-κB complex II translocation in cells cultured with dehydroepiandrosterone and tumor necrosis factor-α, in which the translocation of complex I was not affected [43]. Our results with C6 show that there was an increase in NF-κB translocation of complex I and there was no effect upon complex II translocation. Although it has been described that the p50–p65 heterodimers of NF-κB are involved in enhancing the transcription of target genes and p50–p50 homodimers in transcription repression [44], the biological significance of this difference is not known. It is clear that regulatory proteins, either lipids or adrenal hormones, use different pathways to activate NF-κB dimerization [45,46].

The biological activity of NF-κB is tightly controlled by its inhibitor protein IκB, which binds to and sequesters NF-κB in the cytoplasm. Upon exposure to extracellular signals, a series of biochemical events target the inhibitor protein for degradation, resulting in release and subsequent translocation of NF-κB into the nucleus, where it transactivates the expression of its downstream target genes [47]. We determined whether the increase in the translocation of NF-κB induced by C6 was associated with IκB-α degradation. C6 did not modify the expression

of IκB-α (Fig. 7). Although degradation of IκB proteins in response to stimuli is an obligatory step in NF-κB activation [48], recently it has been shown that the phosphorylation of IκB-α at tyrosine 42 contributes to the activation of NF-κB transcription activity and its phosphorylation at tyrosine 305 is associated with an increase of IκB-α protein stability [49]. It is probable that C6 can induce the phosphorylation at tyrosine 305 of IκB-α and produce its stabilization. When we used an IκB-α kinase inhibitor in combination with C6, C6-induced antiproliferation was not abrogated (Fig. 8), indicating that NF-κB does not participate directly in the C6-induced cell death and that cell death may be a consequence of ROS production induced by C6.

The results obtained in this work suggest that C6 induces the generation of ROS and NO, the loss of mitochondrial membrane potential, the depletion of GSH, and the which activation of NF-κB as a consequence of ROS production, which might be a key step in the initiation of cell death of HPV-positive cervical tumor cells.

Acknowledgements

We thank Dr Mohammed El Hafidi for his help in the determination of GSH concentrations by HPLC.

References

1 Schutze S, Potthoff K, Machleidt T, Berkovic D, Wiegmann K, Kronke M. TNF activates NF-kappa B by phosphatidylcholine-specific phospholipase C-induced 'acidic' sphingomyelin breakdown. *Cell* 1992; **71**:765–776.
2 Wiegmann K, Schutze S, Machleidt T, Witte D, Kronke M. Functional dichotomy of neutral and acidic sphingomyelinases in tumor necrosis factor signaling. *Cell* 1994; **78**:1005–1015.
3 Garcia-Ruiz C, Collel A, Mari M, Morales A, Fernandez-Checa JC. Direct effect of ceramide on the mitochondrial electron transport chain leads to generation of reactive oxygen species. Role of mitochondrial glutathione. *J Biol Chem* 1997; **272**:11369–11377.
4 Rao GN, Glasgow WC, Eling TE, Runge MS. Role of hydroperoxyeicosatetraenoic acids in oxidative stress-induced activating protein 1 (AP-1) activity. *J Biol Chem* 1996; **271**:27760–27764.
5 Quillet-Mary A, Jaffrezou JP, Mansat V, Bordier C, Nava J, Laurent G. Implication of mitochondrial hydrogen peroxide generation in ceramide-induced apoptosis. *J Biol Chem* 1997; **272**:21388–21395.
6 Guarnieri C, Muscari C, Caldarera CM. Mitochondrial production of oxygen free radicals in the heart muscle during the life span of the rat: peak at middle age. *EXS* 1992; **62**:73–77.
7 Arai M, Imai H, Koumura T, Yoshida M, Emoto K, Umeda M, *et al.* Mitochondrial phospholipid hydroperoxide glutathione peroxidase plays a major role in preventing oxidative injury to cells. *J Biol Chem* 1999; **274**:4924–4933.
8 Kaplowitz N, Aw TY, Ookhtens M. The regulation of hepatic glutathione. *Annu Rev Pharmacol Toxicol* 1985; **25**:715–744.
9 Garcia-Ruiz C, Colell A, Morales A, Kaplowitz N, Fernandez-Checa JC. Role of oxidative stress generated from the mitochondrial electron transport chain and mitochondrial glutathione status in loss of mitochondrial function and activation of transcription factor nuclear factor-kappa B: studies with isolated mitochondria and rat hepatocytes. *Mol Pharmacol* 1995; **48**:825–834.
10 Hernandez-Avila M, Lazcano-Ponce EC, de Ruiz PA, Romieu I. Evaluation of the cervical cancer screening programme in Mexico: a population-based case-control study. *Int J Epidemiol* 1998; **27**:370–376.
11 Lopez-Marure R, Gutierrez G, Mendoza C, Ventura JL, Sanchez L, Reyes E, *et al.* Ceramide promotes the death of human cervical tumor cells in the absence of biochemical and morphological markers of apoptosis. *Biochem Biophys Res Commun* 2002; **293**:1028–1036.
12 Monroy A, Rangel R, Rocha L, Trejo C, Ramirez JL, Dario R, *et al.* Obtaining of seven cell lineages derived from biopsies of normal and cancerous cervix and their different content and localization of desmoglein-1. *Oncología* 1992; **7**:69–76.
13 Rangel R, Ramirez JL, Rocha L, Solorza G, Monroy A, Darío R, *et al.* Establishment and characterization of the cell line CaLo and the clone KaLo, derived from a cervical carcinoma, and the effect of IL-2, IL-3, GM-CSF, M-CSF, TNF-α, and IFN-γ on their proliferation. *Rev Inst Nal Cancerol* [in Spanish]. 1993; **39**:1863–1866.
14 Legramandi C, Giannoni R, Barbinni V, Fonte A. Early diagnosis of genito-urinary tumours by urinary cytology. *Arch Ital Urol Nefrol Androl* 1989; **61**:43–46.
15 Sawada GA, Raub TJ, Decker DE, Buxser SE. Analytical and numerical techniques for the evaluation of free radical damage in cultured cells using scanning laser microscopy. *Cytometry* 1996; **25**:254–262.
16 Rothe G, Valet G. Flow cytometric analysis of respiratory burst activity in phagocytes with hydroethidine and 2′,7′-dichlorofluorescin. *J Leukoc Biol* 1990; **47**:440–448.
17 Amano F, Noda T. Improved detection of nitric oxide radical (NO) production in an activated macrophage culture with a radical scavenger, carboxy PTIO and Griess reagent. *FEBS Lett* 1995; **368**:425–428.
18 Haughland RP. *Handbook of fluorescent probes and research chemicals*, 6th ed. Spence MTZ, editor: Molecular Probes; 1996. pp. 531–540.
19 Junqueira V, Carrasquedo F, Azzalis L. Content of liver and brain ubiquinol-9 and ubiquinol-10 after chronic ethanol intake in rats subjected to two levels of dietary tocopherol. *Free Radic Res* 2000; **33**:313–319.
20 Estrada A, Mendoza C, Ventura JL, Lopez LN, Miranda E, Arechavaleta F, *et al.* NF-kappaB dependent activation of human endothelial cells treated with soluble products derived from human lymphomas. *Cancer Lett* 2003; **191**:239–248.
21 Lenardo MJ, Baltimore D. NF-kappa B: a pleiotropic mediator of inducible and tissue-specific gene control. *Cell* 1989; **58**:227–229.
22 Kueng W, Silber E, Eppenberg V. Quantification of cells cultured on 96-well plates. *Anal Biochem* 1989; **186**:16–19.
23 Reynolds CP, Maurer BJ, Kolesnick RN. Ceramide synthesis and metabolism as a target for cancer therapy. *Cancer Lett* 2004; **206**:169–180.
24 Martin D, Salinas M, Fujita N, Tsuruo T, Cuadrado A. Ceramide and reactive oxygen species generated by H_2O_2 induce caspase-3-independent degradation of Akt/protein kinase B. *J Biol Chem* 2002; **277**: 42943–42952.
25 Brovkovych V, Dobrucki LW, Brovkovych S, Dobrucki I, Kalinowski L, Kiechle F, *et al.* Nitric oxide measurements during endotoxemia. *Clin Chem* 2001; **47**:1068–1074.
26 Higuchi Y. Glutathione depletion-induced chromosomal DNA fragmentation associated with apoptosis and necrosis. *J Cell Mol Med* 2004; **8**: 455–464.
27 Wang T, Zhang X, Li JJ. The role of NF-kappaB in the regulation of cell stress responses. *Int Immunopharmacol* 2002; **2**:1509–1520.
28 Haddad JJ. Antioxidant and prooxidant mechanisms in the regulation of redox(y)-sensitive transcription factors. *Cell Signal* 2002; **14**:879–897.
29 Kelly KJ, Sandoval RM, Dunn KW, Molitoris BA, Dagher PC. A novel method to determine specificity and sensitivity of the TUNEL reaction in the quantitation of apoptosis. *Am J Physiol Cell Physiol* 2003; **284**:C1309–C1318.
30 Ramos B, Lahti JM, Claro E, Jackowski S. Prevalence of necrosis in C2-ceramide-induced cytotoxicity in NB16 neuroblastoma cells. *Mol Pharmacol* 2003; **64**:502–511.
31 Phillips DC, Allen K, Griffiths HR. Synthetic ceramides induce growth arrest or apoptosis by altering cellular redox status. *Arch Biochem Biophys* 2002; **407**:15–24.
32 Kim WH, Choi CH, Kang SK, Kwon CH, Kim YK. Ceramide induces non-apoptotic cell death in human glioma cells. *Neurochem Res* 2005; **30**:969–979.
33 Chung HT, Pae HO, Choi BM, Billiar TR, Kim YM. Nitric oxide as a bioregulator of apoptosis. *Biochem Biophys Res Commun* 2001; **282**:1075–1079.
34 Choi BM, Pae HO, Jang SI, Kim YM, Chung HT. Nitric oxide as a pro-apoptotic as well as anti-apoptotic modulator. *J Biochem Mol Biol* 2002; **35**:116–126.
35 Trulsson LM, Gasslander T, Svanvik J. Cholecystokinin-8-induced hypoplasia of the rat pancreas: influence of nitric oxide on cell proliferation and programmed cell death. *Basic Clin Pharmacol Toxicol* 2004; **95**:183–190.
36 Lavrentiadou SN, Chen C, Kawcak T, Ravid T, Tsaba A, Van der Vliet A, *et al.* Ceramide-mediated apoptosis in lung epithelial cells is regulated by glutathione. *Am J Respir Cell Mol Biol* 2001; **25**:676–684.
37 Fernandez-Checa JC, Garcia-Ruiz C, Colellm A, Morales A, Mari M, Miranda M, *et al.* Oxidative stress: role of mitochondria and protection by glutathione. *Biofactors* 1998; **8**:7–11.

38 Goldkorn T, Ravid T, Khan EM. Life and death decisions: ceramide generation and EGF receptor trafficking are modulated by oxidative stress. *Antioxid Redox Signal* 2005; **7**:119–128.
39 Garcia-Ruiz C, Mari M, Morales A, Colell A, Ardite E, Fernadez-Checa JC. Human placenta sphingomyelinase, an exogenous acidic pH-optimum sphingomyelinase, induces oxidative stress, glutathione depletion, and apoptosis in rat hepatocytes. *Hepatology* 2000; **32**:56–65.
40 Schutze S, Wiegmann K, Machleidt T, Kronke M. TNF-induced activation of NF-kappa B. *Immunobiology* 1995; **193**:193–203.
41 Fillet M, Bentires-Alj M, Deregowski V, Greimers R, Gielen J, Piette J, *et al.* Mechanisms involved in exogenous C2- and C6-ceramide-induced cancer cell toxicity. *Biochem Pharmacol* 2003; **65**:1633–1642.
42 Ghosh S, Bhattacharyya S, Sirkar M, Sa GS, Das T, Majumdar D, *et al.* Leishmania donovani suppresses activated protein 1 and NF-kappaB activation in host macrophages via ceramide generation: involvement of extracellular signal-regulated kinase. *Infect Immun* 2002; **70**:6828–6838.
43 Gutierrez G, Mendoza C, Zapata E, Montiel A, Reyes E, Montaño LF, *et al.* Dehydroepiandrosterone inhibits the TNF-alpha-induced inflammatory response in human umbilical vein endothelial cells. *Atherosclerosis* 2006 [Epub ahead of print)]
44 Udalova IA, Richardson A, Denys A, Smith C, Ackerman H, Foxwell B, *et al.* Functional consequences of a polymorphism affecting NF-kappaB p50–p50 binding to the TNF promoter region. *Mol Cell Biol* 2000; **20**:9113–9119.
45 Cohen L, Hiscott J. Heterodimerization and transcriptional activation in vitro by NF-kappa B proteins. *J Cell Physiol* 1992; **152**:10–18.
46 Caldenhoven E, Liden J, Wissink S, Van de Stolpe A, Raaijmakers J, Koenderman L, *et al.* Negative cross-talk between RelA and the glucocorticoid receptor: a possible mechanism for the antiinflammatory action of glucocorticoids. *Mol Endocrinol* 1995; **9**:401–412.
47 Huang TT, Miyamoto S. Postrepression activation of NF-κB requires the amino-terminal nuclear export signal specific to IkBα. *Mol Cell Biol* 2001; **21**:4737–4747.
48 Karin M, Ben-Neriah Y. Phosphorylation meets ubiquitination: the control of NF-κB activity. *Annu Rev Immunol* 2000; **18**:621–663.
49 Kawai H, Nie L, Yuan ZM. Inactivation of NF-κB-dependent cell survival, a novel mechanism for the proapoptotic function of c-Abl. *Mol Cell Biol* 2002; **22**:6079–6088.